Multibody Syst Dyn (2018) 43:279–295
DOI 10.1007/s11044-017-9598-z

Dynamics analysis and fuzzy anti-swing control design of overhead crane system based on Riccati discrete time transfer matrix method

Bao Rong[1] · Xiaoting Rui[2] · Ling Tao[1] · Guoping Wang[2]

Received: 15 February 2017 / Accepted: 9 October 2017 / Published online: 25 October 2017

Abstract This paper describes an efficient method called Riccati discrete time transfer matrix method of multibody system (MS-RDTTMM) for studying the dynamic modeling and anti-swing control design of a two-dimensional overhead crane system, which consists of a trolley, rope, load, and control subsystem. Regarding the rope as a series of rigid segments connected by hinges, a multibody model of the overhead crane system can be developed easily by using MS-RDTTMM. Then three separate fuzzy logic controllers are designed for positioning and anti-swing control. For improving the performance of the predesigned fuzzy control system, the genetic algorithm based on MS-RDTTMM is presented offline to tune the initial control parameters. Using the recursive transfer formula to describe the system dynamics, instead of the global dynamics equation in ordinary dynamics methods, the matrices involved in this method are always very small, and the computational cost of the dynamic analysis and control system optimization can be greatly reduced. The numerical verification is carried out to show the computational efficiency, numerical stability, and control performance of the proposed method.

Keywords Multibody system dynamics · Discrete time transfer matrix method · Fuzzy control · Overhead crane · Genetic algorithm

1 Introduction

Overhead crane plays an important role in many factories and harbors, which transports a load from one place to another. Crane acceleration, deceleration, and disturbances always induce undesirable load swing, and decrease the crane performance. Such problems decrease the work efficiency and in some cases cause damage to the loads and cause safety accidents [1–4]. As the high positioning accuracy, small swing angle, short transportation

✉ L. Tao
palytao@ipp.ac.cn

1 Institute of Plasma Physics, Chinese Academy of Sciences (ASIPP), Hefei 230031, P.R. China

2 Institute of Launch Dynamics, Nanjing University of Science and Technology, Nanjing 210094, P.R. China

time, and high safety are required, operating an overhead crane is hard work, and various attempts have been made to control the load swing and the trolley position, which is often not a simple task since an overhead crane has fewer control inputs than its degrees of freedom (DOF). Lee (2001) used the fuzzy logic anti-swing controller and position servo controller for positioning and swing damping [5]. Karkoub (2002) developed modeling and energy based nonlinear control for crane lifters [6]. Matsuo (2004) used the PID+Q-based controller to minimize the crane sway [3]. Fang (2003) employed a dynamic crane model to determine an optimal speed that minimized load swing [7]. Liu (2005) used Lagrange method for dynamic modeling of a two-dimensional overhead crane, and then proposed an adaptive sliding mode fuzzy control approach for anti-swing control [8]. Chang (2008) studied fuzzy projection control law and its application to the overhead crane [2]. Park (2008) presented an adaptive fuzzy sliding-mode control for the robust anti-swing trajectory tracking of overhead cranes subject to both system uncertainty and actuator nonlinearity [4]. Yu (2011) proposed a novel fast control strategy including a normal proportional and derivative regulator and a fuzzy cerebellar model articulation controller to realize position tracking and anti-swing of an overhead crane [9]. Tuan (2013) studied an adaptive sliding mode control of a crane system in the case of no prior knowledge of the payload mass and damped elements [10]. Pezeshki (2015) employed a model-free adaptive controller using feedback linearization and an adaptive fuzzy sliding mode controller using fuzzy approximation to control an underactuated overhead crane system [11]. Zhang (2017) considered a finite-time regulation controller for 2-dimensional underactuated crane system with both constant and varying cable length [12].

The nonlinear crane system is a controlled multibody system essentially, which consists of a trolley, rope, load, and other components interacting with some control subsystems. In general, when studying dynamics and control design of a controlled crane system, one must establish the global dynamics equations firstly by using multibody dynamics methods [13–17], such as Wittenburg, Kane, Lagrange, and so on. Then based on that, various control methods can be attempted to design the crane control system. As the order of the global dynamics equations by ordinary dynamics methods increases with the DOF of the system, the computational cost of high-DOF model would be expensive and it is difficult to satisfy the real-time control. Thus, for solving the problem of computational consumption and real-time control, most existing literature sources often have to adopt reduced crane system model to deal with its dynamics and control design. For example, the dynamics of rope in a crane system is quite complex and difficult, and its dynamics model can be usually described by the continuum models or by some discrete modeling methods, such as finite segment, finite element, and so on. Then the dynamic equations of rope can be written as the complex partial differential equations or differential equations, and the computational cost for solving these dynamic equations is very high, especially when using the discrete modeling methods to study the rope dynamics. So in order to improve the computational efficiency, when deducing the dynamic equations of overhead crane system, most existing literature takes no account of the effect of rope on dynamics and control [1, 2]. However, the reduced dynamic model is sometimes difficult to reflect the dynamic performance of the real system, and leads to low accuracy or even instability of control system.

The transfer matrix method (TMM), which doesn't need the system global dynamic equations and has low system matrix order [18], has been used widely in structure mechanics and rotor dynamics for the purpose of saving computational cost. Rui et al. (2005, 2010) presented the discrete time TMM of multibody system (MS-DTTMM) to study general multibody dynamics [19, 20]. For different dynamics problems, He (2007), Wang (2012), and Rong (2014) introduced Riccati transform to improve the numerical stability of TMM

[21–23]. This method provides a potential means for efficient dynamics modeling and control design of complex crane systems.

In this paper, combining the MS-DTTMM and Riccati transform technology, an efficient method called Riccati discrete time transfer matrix method of multibody system (MS-RDTTMM) is presented to study the dynamic modeling and control design of a two-dimensional overhead crane system. Three separate fuzzy logic controllers are predesigned for positioning and anti-swing control, and their control parameters are tuned offline by genetic algorithm (GA) based on MS-RDTTMM. Some numerical simulations will show that the proposed method is a very useful method for dynamic analysis and control system optimization of controlled crane systems because of its simplicity and numerical efficiency.

2 Dynamic modeling of two-dimensional overhead crane system by MS-RDTTMM

As shown in Fig. 1, the two-dimensional overhead crane is regarded as a nonlinear underactuated multibody system, and consists of a trolley, rope, load, and control subsystem. A servomotor is used to control the trolley position and the load swing. For convenience, rope elasticity and rail friction are ignored, and the rope length is usually kept constant when the overhead crane is in motion. In this study, trolley and load are regarded as rigid bodies. The rope is modeled as a series of rigid segments connected by smooth hinges [24–26]. As Kamman and Huston (2001) pointed out, the multibody modeling of the rope has distinct advantages over traditional continuum rope models, because the nonlinear and large-motion effects of the rope can be studied conveniently with multibody models [24]. The numbers $1 \sim (2n+3)$ in Fig. 1 denote the serial numbers of elements. n is the total number of the rope's segments. Combining the MS-DTTMM and Riccati transform technology, by deducing new transfer equations of controlled elements, an efficient MS-RDTTMM will be presented for dynamics modeling of the controlled crane system in this section.

2.1 Linearization of dynamic equations of elements

As the transfer equation and transfer matrix of each element used in our method are obtained by linearizing its dynamics equations, the common linearization methods need to be simply introduced first in order to facilitate reader understanding, and their details can be seen in [19–22]. The motion parameters $\ddot{\boldsymbol{\xi}}$ and $\dot{\boldsymbol{\xi}}$ in the dynamic equations of each element at time t_i [19–22] are expressed as

$$\ddot{\boldsymbol{\xi}}(t_i) = \boldsymbol{\chi}_1 \boldsymbol{\xi}(t_i) + \boldsymbol{\chi}_{2,\xi}, \qquad \dot{\boldsymbol{\xi}}(t_i) = \boldsymbol{\chi}_3 \boldsymbol{\xi}(t_i) + \boldsymbol{\chi}_{4,\xi} \tag{1}$$

where $\boldsymbol{\xi}$ denotes the position coordinates x, y or orientation angle θ; $\dot{\boldsymbol{\xi}}$ and $\ddot{\boldsymbol{\xi}}$ are the first and second derivatives of $\boldsymbol{\xi}$ with respect to time. $\boldsymbol{\chi}_1$, $\boldsymbol{\chi}_{2,\xi}$, $\boldsymbol{\chi}_3$, and $\boldsymbol{\chi}_{4,\xi}$ will have different expressions for different numerical integration methods. For Newmark-β method [27], they can be expressed as:

$$\boldsymbol{\chi}_1 = \frac{1}{\beta \Delta T^2}\mathbf{I}_k, \qquad \boldsymbol{\chi}_{2,\xi} = -\frac{1}{\beta \Delta T^2}\left[\boldsymbol{\xi}(t_{i-1}) + \Delta T \dot{\boldsymbol{\xi}}(t_{i-1}) + \left(\frac{1}{2} - \beta\right)\Delta T^2 \ddot{\boldsymbol{\xi}}(t_{i-1})\right], \tag{2}$$

$$\boldsymbol{\chi}_3 = \gamma \boldsymbol{\chi}_1 \Delta T, \qquad \boldsymbol{\chi}_{4,\xi} = \dot{\boldsymbol{\xi}}(t_{i-1}) + \Delta T\left[(1-\gamma)\ddot{\boldsymbol{\xi}}(t_{i-1}) + \gamma \boldsymbol{\chi}_{2,\xi}\right]. \tag{3}$$

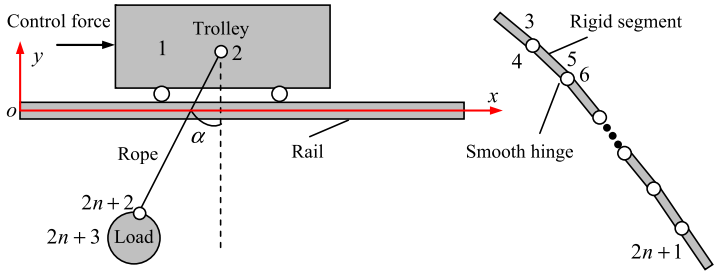

(a) Overhead crane system (b) Discrete rope dynamic model

Fig. 1 Controlled overhead crane system and rope dynamic model

$\Delta T = t_i - t_{i-1}$ is the time step, β and γ are the coefficients of Newmark-β method. Bold capital symbol $\mathbf{I}_k$ is the unit matrix, and the subscript k denotes its order. If $\gamma \geq 1/2$ and $\beta \geq \gamma/2$, the formulas are unconditionally stable.

Based on the Taylor expansion, the trigonometric functions and multinomial [19–22] in the dynamic equations of each element at time t_i can be expressed as

$$\begin{aligned} \sin\theta(t_i) &= \cos\theta(t_{i-1})\theta(t_i) + G_2 + o\big(\Delta T^2\big), \\ \cos\theta(t_i) &= -\sin\theta(t_{i-1})\theta(t_i) + G_1 + o\big(\Delta T^2\big), \end{aligned} \tag{4}$$

$$a(t_i)b(t_i) = a(t_{i-1})b(t_i) + a(t_i)b(t_{i-1}) - a(t_{i-1})b(t_{i-1}) + \dot{a}(t_{i-1})\dot{b}(t_{i-1})\Delta T^2 \tag{5}$$

where

$$\begin{aligned} G_1 &= \cos\theta(t_{i-1}) + \theta(t_{i-1})\sin\theta(t_{i-1}) - \frac{1}{2}\cos\theta(t_{i-1})\big[\dot{\theta}(t_{i-1})\Delta T\big]^2, \\ G_2 &= \sin\theta(t_{i-1}) - \theta(t_{i-1})\cos\theta(t_{i-1}) - \frac{1}{2}\sin\theta(t_{i-1})\big[\dot{\theta}(t_{i-1})\Delta T\big]^2. \end{aligned} \tag{6}$$

$\boldsymbol{\xi}(t_{i-1})$, $\dot{\boldsymbol{\xi}}(t_{i-1})$, and $\ddot{\boldsymbol{\xi}}(t_{i-1})$ are all known at time t_i. Thus, the quantities $\boldsymbol{\chi}_1$, $\boldsymbol{\chi}_{2,\xi}$, $\boldsymbol{\chi}_3$, $\boldsymbol{\chi}_{4,\xi}$, $\bar{s}$, $\bar{c}$, etc., are all definable for any element at time t_i, and hence the above formulations are valid [19–22].

2.2 State vector, transfer equation and transfer matrix of each element

For the multibody model of the two-dimensional overhead crane system shown in Fig. 1, one can define the state vector of connection point between any rigid body and hinge [19, 20] as

$$\mathbf{z} = [x, y, \theta, m, q_x, q_y, 1]^{\mathrm{T}} \tag{7}$$

where m, q_x, and q_y are the interior moment and interior forces of the connection point with respect to the inertial reference system, respectively.

2.2.1 Transfer matrix of controlled rigid body moving in a plane

A rigid body moving in a plane with control moment and control force is shown in Fig. 2. Points I, O, and C denote the inboard point, outboard point, and mass center of rigid body, respectively; $O_2x_2y_2$ is the body-fixed reference system whose origin O_2 is on point I,

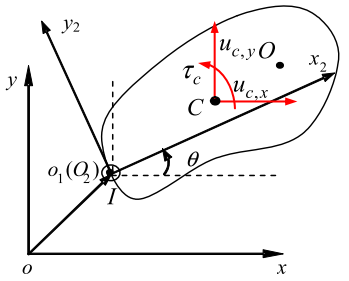

Fig. 2 Rigid body moving in plane with control

oxy is the inertial reference system. $(b_{p,1}, b_{p,2})$ are the position coordinates of point p with respect to the body-fixed reference system. For any point p, the following geometrical equations can be obtained:

$$x_p = x_I + x_{Ip}, \qquad y_p = y_I + y_{Ip}, \qquad \theta_p = \theta \tag{8}$$

where (x_p, y_p) are the position coordinates of point p with respect to the inertial reference system. $x_{Ip} = b_{p,1}c_I - b_{p,2}s_I$, $y_{Ip} = b_{p,1}s_I + b_{p,2}c_I$, $s_I = \sin\theta_I$, and $c_I = \cos\theta_I$.

The dynamic equations of the controlled rigid body moving in a plane [19–22] can be obtained as

$$m\ddot{x}_C = q_{x,I} - q_{x,O} + f_{x,C} + u_{c,x}, \qquad m\ddot{y}_C = q_{y,I} - q_{y,O} + f_{y,C} + u_{c,y}, \tag{9}$$

$$\begin{aligned} J_I\ddot{\theta}_I + mx_{IC}\ddot{y}_I - my_{IC}\ddot{x}_I = {} & m_O - m_I + m_C + q_{x,O}y_{IO} \\ & - q_{y,O}x_{IO} - f_{x,C}y_{IC} + f_{y,C}x_{IC} + \tau_C \end{aligned} \tag{10}$$

where m is the mass of rigid body, $q_{x,I}$, $q_{y,I}$ are the internal forces of the inboard point, $q_{x,O}$, $q_{y,O}$ are the internal forces of the outboard point, m_I, m_O are the internal moments of the inboard and outboard points, respectively, $f_{x,C}$, $f_{y,C}$, and m_C are the external forces and external moment acted on mass center. J_I is the moment of inertia with respect to point I; $u_{C,x}$, $u_{C,y}$, and τ_C are the control forces and control moment acted on mass center, respectively. These control moment and control forces can be designed by the corresponding control law. For the two-dimensional overhead crane shown in Fig. 1, the controlled trolley moves along a rail, and only control force $u_{C,x}$ is considered, which will be described in Sect. 3.

Linearizing Eq. (8) by Eq. (4), then one obtains

$$\begin{aligned} x_O &= x_I - y_{IO}(t_{i-1})\theta_I + b_{O,1}G_1 - b_{O,2}G_2, \\ y_O &= y_I + x_{IO}(t_{i-1})\theta_I + b_{O,1}G_2 + b_{O,2}G_1. \end{aligned} \tag{11}$$

Substituting Eq. (8) into Eq. (9), and linearizing by using Eqs. (1) and (4), one gets

$$q_{x,O} = -m\chi_1 x_I + m\chi_1 y_{IC}(t_{i-1})\theta_I + q_{x,I} + u_{57} + u_{c,x}, \tag{12}$$

$$q_{y,O} = -m\chi_1 y_I - m\chi_1 x_{IC}(t_{i-1})\theta_I + q_{y,I} + u_{67} + u_{c,y}. \tag{13}$$

Substituting Eqs. (12) and (13) into Eq. (10), and linearizing by using Eq. (1), one obtains

$$m_O = u_{41}x_I + u_{42}y_I + u_{43}\theta_I + m_I + u_{45}q_{x,I} + u_{46}q_{y,I} + u_{47} + \tau_C. \tag{14}$$

Define the control input acted on the controlled rigid body as

$$\mathbf{u}_C = [u_{c,x}, \quad u_{c,y}, \quad \tau_c, 1]^{\mathrm{T}}. \tag{15}$$

Combining Eqs. (8), (11)–(14), the transfer equation of planar controlled rigid body [19–22] is obtained as

$$\mathbf{z}_O = \mathbf{U}\mathbf{z}_I + \mathbf{H}\mathbf{u}_C. \tag{16}$$

Transfer matrices are

$$\mathbf{U} = \begin{bmatrix} 1 & 0 & -y_{IO}(t_{i-1}) & 0 & 0 & 0 & b_{O,1}G_1 - b_{O,2}G_2 \\ 0 & 1 & x_{IO}(t_{i-1}) & 0 & 0 & 0 & b_{O,1}G_2 + b_{O,2}G_1 \\ 0 & 0 & 1 & 0 & 0 & 0 & 0 \\ u_{41} & u_{42} & u_{43} & 1 & u_{45} & u_{46} & u_{47} \\ -m\chi_1 & 0 & m\chi_1 y_{IC}(t_{i-1}) & 0 & 1 & 0 & u_{57} \\ 0 & -m\chi_1 & -m\chi_1 x_{IC}(t_{i-1}) & 0 & 0 & 1 & u_{67} \\ 0 & 0 & 0 & 0 & 0 & 0 & 1 \end{bmatrix},$$

$$\mathbf{H} = \begin{bmatrix} 0 & 0 & 0 & 0 \\ 0 & 0 & 0 & 0 \\ 0 & 0 & 0 & 0 \\ 0 & 0 & -1 & 0 \\ 1 & 0 & 0 & 0 \\ 0 & 1 & 0 & 0 \\ 0 & 0 & 0 & 0 \end{bmatrix} \tag{17}$$

where the state vectors $\mathbf{z}_I$ and $\mathbf{z}_O$ are defined as in Eq. (7):

$$\begin{aligned} &u_{41} = m\chi_1(y_{IO} - y_{IC}), \qquad u_{42} = m\chi_1(x_{IO} - x_{IC}), \\ &u_{43} = -m\chi_1 x_{IC}(t_{i-1})x_{IO} - m\chi_1 y_{IC}(t_{i-1})y_{IO} + J_I\chi_1, \\ &u_{45} = -y_{IO}, \\ &u_{47} = -m_C + u_{67}x_{IO} - u_{57}y_{IO} + J_I\chi_{2,\theta} + (m\chi_{2,y_I} - f_{y,C})x_{IC} + (f_{x,C} - m\chi_{2,x_I})y_{IC}, \\ &u_{46} = x_{IC}, \qquad u_{57} = f_{x,C} - m\chi_1(b_{C,1}G_1 - b_{C,2}G_2) - m\chi_{2,x_C}, \\ &u_{67} = f_{y,C} - m\chi_1(b_{C,1}G_2 + b_{C,2}G_1) - m\chi_{2,y_C}, \\ &x_{Ip}(t_{i-1}) = (b_{p,1}c_I - b_{p,2}s_I)\big|_{t_{i-1}}, \qquad y_{Ip}(t_{i-1}) = (b_{p,1}s_I + b_{p,2}s_I)\big|_{t_{i-1}}. \end{aligned} \tag{18}$$

Especially, for the discrete rope model shown as Fig. 1(b), each rigid segment can be regarded as a rigid body moving in plane without control, so according to Eq. (16), the transfer equation of each rigid segment moving in plane without control can be obtained as

$$\mathbf{z}_O = \mathbf{U}\mathbf{z}_I. \tag{19}$$

Here, the transfer matrix $\mathbf{U}$ has the same form as Eq. (17).

2.2.2 *Transfer matrix of smooth pin hinge*

The model of smooth pin hinge [19–22] is shown in Fig. 3. The symbols I and O denote the inboard and outboard ends of a smooth pin hinge j, respectively, and $j-1$ and $j+1$

Fig. 3 Smooth pin hinge model

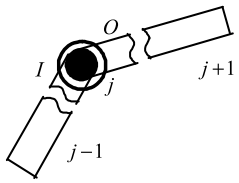

denote its inboard body and outboard body, respectively. Neglecting the mass and size of a smooth pin hinge, one gets

$$x_O = x_I, \qquad y_O = y_I, \qquad q_{y,O} = q_{y,I}, \qquad q_{x,O} = q_{x,I}, \qquad m_O = m_I = 0. \tag{20}$$

If the outboard end of the outboard rigid body connects smooth pin hinge or has free boundary, from the transfer equation of outboard rigid body of smooth pin hinge, one can obtain

$$0 = u_{41}x_O + u_{42}y_O + u_{43}\theta_O + u_{45}q_{x,O} + u_{46}q_{y,O} + u_{47} \tag{21}$$

where u_{41}, u_{42}, u_{43}, u_{45}, u_{46}, u_{47} are elements of the transfer matrix of outboard rigid body, shown as Eq. (18).

Combining Eqs. (20) and (21), the transfer equation of the smooth pin hinge [19–22] can be obtained as

$$\mathbf{z}_O = \mathbf{U}\mathbf{z}_I \tag{22}$$

with the transfer matrix

$$\mathbf{U} = \begin{bmatrix} 1 & 0 & 0 & 0 & 0 & 0 & 0 \\ 0 & 1 & 0 & 0 & 0 & 0 & 0 \\ -\frac{u_{41}}{u_{43}} & -\frac{u_{42}}{u_{43}} & 0 & 0 & -\frac{u_{45}}{u_{43}} & -\frac{u_{46}}{u_{43}} & -\frac{u_{47}}{u_{43}} \\ 0 & 0 & 0 & 0 & 0 & 0 & 0 \\ 0 & 0 & 0 & 0 & 1 & 0 & 0 \\ 0 & 0 & 0 & 0 & 0 & 1 & 0 \\ 0 & 0 & 0 & 0 & 0 & 0 & 1 \end{bmatrix}. \tag{23}$$

The state vectors $\mathbf{z}_I$ and $\mathbf{z}_O$ are defined as in Eq. (7).

2.3 Dynamics solution of the controlled overhead crane system

From Eqs. (16), (19), and (23), the following transfer equations of elements can be obtained

$$\mathbf{z}_{O,P} = \begin{cases} \mathbf{U}_P\mathbf{z}_{I,p} + \mathbf{H}_p\mathbf{u}_C & (p = 1), \\ \mathbf{U}_P\mathbf{z}_{I,P} & (p = 2, 3, \ldots, 2n+3), \end{cases} \tag{24}$$

where the subscript p denotes the serial number of the element. $\mathbf{U}_1$ and $\mathbf{H}_1$ are the transfer matrices of controlled trolley 1, defined by Eq. (17); $\mathbf{U}_2$ is the transfer matrix of smooth hinge 2, defined by Eq. (23); $\mathbf{U}_{2n+3}$ is the transfer matrix of load $2n+3$, defined by Eq. (19). n is the number of the rope segments. $\mathbf{U}_{2i+1}$ and $\mathbf{U}_{2i+2}$ $(i = 1, 2, \ldots, n)$ are the transfer matrices of rigid segment $(2i+1)$ and smooth hinge $(2i+2)$, defined by Eqs. (19) and (23), respectively.

When using the ordinary MS-DTTMM [19], considering Eq. (24), the overall transfer equation of the controlled crane system shown in Fig. 1 can be assembled as

$$\mathbf{z}_{O,2n+3} = \mathbf{U}_{2n+3}\prod_{i=1}^{n}\left(\mathbf{U}_{2i+2}\mathbf{U}_{2i+1}\right)\mathbf{U}_2\mathbf{U}_1\mathbf{z}_{I,1} + \mathbf{U}_{2n+3}\prod_{i=1}^{n}(\mathbf{U}_{2i+2}\mathbf{U}_{2i+1})\mathbf{U}_2\mathbf{H}_1\mathbf{u}_C. \tag{25}$$

Applying the boundary conditions of a system into Eq. (25), considering transfer Eqs. (24) of elements and numerical integration expression (1), all motion quantities at time t_i can be obtained. Then the entire procedure can be repeated for time t_{i+1}, and so on [19, 22]. As pointed out in [21, 22], recursive multiplication of transfer matrices leads to the propagation of round-off errors by the ordinary MS-DTTMM, and if the number of rope segments is large, numerical instability will appear. For solving this problem, the following Riccati transform technology [21, 22] is introduced.

Rearrange the state vector (7) into three parts as

$$\mathbf{z} = \left[\mathbf{z}_a^{\mathrm{T}}, \quad \mathbf{z}_b^{\mathrm{T}}, \quad 1\right]^{\mathrm{T}} \tag{26}$$

where $\mathbf{z}_a$ and $\mathbf{z}_b$ include the known and unknown state variables in the inboard boundary of system, respectively. For the crane system shown in Fig. 1, one can let $\mathbf{z}_a = [y,\ \theta,\ q_x]^{\mathrm{T}}$ and $\mathbf{z}_b = [x,\ m,\ q_y]^{\mathrm{T}}$.

Thus, Eq. (24) can be rearranged as

$$\begin{aligned}
\begin{bmatrix}\mathbf{z}_a\\ \mathbf{z}_b\end{bmatrix}_{O,p} &= \begin{bmatrix}\bar{\mathbf{U}}_{11} & \bar{\mathbf{U}}_{12}\\ \bar{\mathbf{U}}_{21} & \bar{\mathbf{U}}_{22}\end{bmatrix}_p \begin{bmatrix}\mathbf{z}_a\\ \mathbf{z}_b\end{bmatrix}_{I,p} + \begin{bmatrix}\bar{\mathbf{H}}_a\\ \bar{\mathbf{H}}_b\end{bmatrix}_p \mathbf{u}_C + \begin{bmatrix}\bar{\mathbf{U}}_{13}\\ \bar{\mathbf{U}}_{23}\end{bmatrix}_p \quad (p=1),\\
\begin{bmatrix}\mathbf{z}_a\\ \mathbf{z}_b\end{bmatrix}_{O,p} &= \begin{bmatrix}\bar{\mathbf{U}}_{11} & \bar{\mathbf{U}}_{12}\\ \bar{\mathbf{U}}_{21} & \bar{\mathbf{U}}_{22}\end{bmatrix}_p \begin{bmatrix}\mathbf{z}_a\\ \mathbf{z}_b\end{bmatrix}_{I,p} + \begin{bmatrix}\bar{\mathbf{U}}_{13}\\ \bar{\mathbf{U}}_{23}\end{bmatrix}_p \quad (p=2,3,\ldots,2n+3).
\end{aligned} \tag{27}$$

Based on the partition of $\mathbf{z}_a$ and $\mathbf{z}_b$, $\bar{\mathbf{U}}_{jk}$ $(j=1,2;\ k=1,2,3)$, $\bar{\mathbf{H}}_a$, and $\bar{\mathbf{H}}_b$ can be obtained easily.

Letting

$$\mathbf{P}_p = (\bar{\mathbf{U}}_{21,p}\mathbf{S}_p + \bar{\mathbf{U}}_{22,p})^{-1}, \qquad \mathbf{Q}_p = -(\bar{\mathbf{U}}_{21,p}\mathbf{e}_p + \bar{\mathbf{U}}_{23,p}) \tag{28}$$

and substituting the Riccati transform [21, 22]

$$\mathbf{z}_{a(I,p)} = \mathbf{S}_p\mathbf{z}_{b(I,p)} + \mathbf{e}_p \quad (p=1,2,\ldots,2n+3) \tag{29}$$

into Eq. (27), one obtains

$$\begin{aligned}
\mathbf{z}_{b(I,p)} &= \begin{cases}\mathbf{P}_p\mathbf{z}_{b(O,p)} + \mathbf{P}_p\mathbf{Q}_p - \mathbf{P}_p\bar{\mathbf{H}}_{b,p}\mathbf{u}_C & (p=1),\\ \mathbf{P}_p\mathbf{z}_{b(O,p)} + \mathbf{P}_p\mathbf{Q}_p & (p=2,3,\ldots,2n+3),\end{cases}\\
\mathbf{z}_{a(I,p+1)} &= \mathbf{S}_{p+1}\mathbf{z}_{b(I,p+1)} + \mathbf{e}_{p+1}
\end{aligned} \tag{30}$$

where the following recursive formula holds:

$$\begin{aligned}
\mathbf{S}_{p+1} &= (\bar{\mathbf{U}}_{11,p}\mathbf{S}_p + \bar{\mathbf{U}}_{12,p})\mathbf{P}_p,\\
\mathbf{e}_{p+1} &= \begin{cases}\bar{\mathbf{U}}_{11,p}\mathbf{e}_p + \bar{\mathbf{U}}_{13,p} + \mathbf{S}_{p+1}\mathbf{Q}_p + [\bar{\mathbf{H}}_{a,p} - \mathbf{S}_{p+1}\bar{\mathbf{H}}_{b,p}]\mathbf{u}_C & (p=1),\\ \bar{\mathbf{U}}_{11,p}\mathbf{e}_p + \bar{\mathbf{U}}_{13,p} + \mathbf{S}_{p+1}\mathbf{Q}_p & (p=2,3,\ldots,2n+3).\end{cases}
\end{aligned} \tag{31}$$

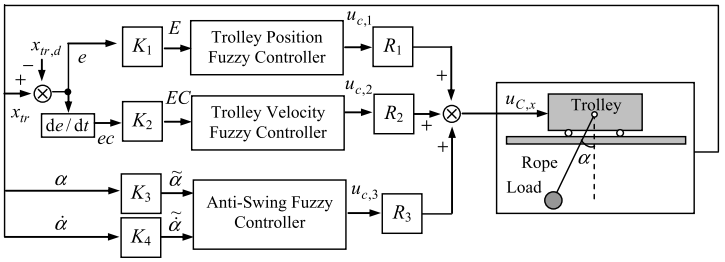

Fig. 4 Control block diagram of the controlled crane system

As the input boundary conditions of system are $\mathbf{z}_{a(I,1)} = \mathbf{0}$ and $\mathbf{z}_{b(I,1)} \neq \mathbf{0}$, the starting condition of Eq. (31) is

$$\mathbf{S}_1 = \mathbf{0}, \qquad \mathbf{e}_1 = \mathbf{0}. \tag{32}$$

By using Eq. (31) repeatedly, the matrix $\mathbf{S}$ and $\mathbf{e}$ at any connection point can be obtained, especially at the output boundary point of system

$$\mathbf{z}_{a(O,2n+3)} = \mathbf{S}_{2n+4}\mathbf{z}_{b(O,2n+3)} + \mathbf{e}_{2n+4}. \tag{33}$$

The unknown state variables of the output boundary point of system at time t_i can be obtained by solving the algebraic Eq. (33). Then by Eq. (31), the state vectors of any connection point at time t_i can be obtained. The velocity, angular velocity, acceleration, and angular acceleration quantities at time t_i are obtained by numerically integrating Eq. (1). Then the entire procedure can be repeated for time t_{i+1} until to the required time. This method avoids solving the global stiff differential or differential-algebraic equations which have too high matrix orders if the number of DOF of the system is large (especially, when using ordinary dynamics methods), and only needs to solve the algebraic recursive transfer equations, thus simplifying the algorithm of dynamics analysis. Moreover, the order of matrices involved in this method is independent of the number of DOF of the system, only (3×3) for planar chain controlled multibody system dynamics, which greatly improves the computational efficiency.

3 Control strategy

The overhead crane control is a problem with two objectives: trolley positioning and payload anti-swing. The control objective is to drive the trolley to transport the load safely from an initial position to the destination in short time without residual swing. In this section, a nonlinear fuzzy control strategy is proposed to control the crane. Generally, when designing a fuzzy controller, the error variables and their differentials are often applied to be the antecedent parts of the fuzzy controller. However, for a multivariate fuzzy control system, this simple design would result in complicated fuzzy rules and huge time cost [28, 29]. Suppose that the trolley position x_{tr}, trolley velocity $\dot{x}_{tr}$, swing angle α, and swing angular velocity $\dot{\alpha}$, which were all divided into five fuzzy linguistic sets, were selected as the input variables of a fuzzy controller, then we would need 5^4 rules to fulfill a fuzzy controller, which would reduce the computational efficiency [1, 2]. Here, the swing angle α is the angle between the plumb line and the line connecting the load centroid and the hanging point of the trolley.

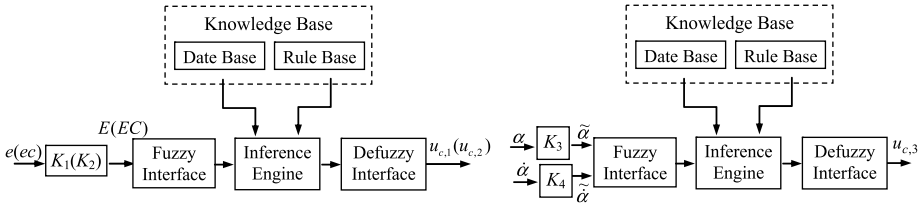

(a) Trolley position (or velocity) fuzzy controller (b) Anti-swing fuzzy controller

Fig. 5 Basic structures of fuzzy controllers

In order to improve the efficiency of the fuzzy controller and realize the high-performance control of load swing and crane position, the following fuzzy control method [29] shown in Fig. 4 is presented. In this fuzzy control method, three separate fuzzy controllers (trolley position fuzzy controller, trolley velocity fuzzy controller, and anti-swing fuzzy controller) are designed for controlling the load swing and crane position. The total control force $u_{C,x}$ acted on the trolley is obtained by

$$u_{C,x} = R_1 u_{C,1} + R_2 u_{C,2} + R_3 u_{C,3} \tag{34}$$

where $u_{C,1}$, $u_{C,2}$, and $u_{C,3}$ are the control outputs of the trolley position fuzzy controller, trolley velocity fuzzy controller, and anti-swing fuzzy controller, respectively. R_1, R_2, and R_3 are the scale factors.

3.1 Design of each fuzzy controller

The basic structures of the trolley position fuzzy controller, trolley velocity fuzzy controller, and anti-swing fuzzy controller [29] are shown in Fig. 5. The trolley position error e and its derivative ec are used to be the input variables of the trolley position fuzzy controller and trolley velocity fuzzy controller, respectively. The swing angle α and swing angular velocity $\dot{\alpha}$ are used to be the input variables of the anti-swing fuzzy controller. K_1, K_2, K_3, and K_4 are the quantization factors. The dynamic ranges of variables E, EC, $\tilde{\alpha}$, $\tilde{\dot{\alpha}}$, $u_{c,1}$, $u_{c,2}$, and $u_{c,3}$ are all $[-4,\ 4]$. The fuzzier is a mapping from a real-valued point to a fuzzy set. In a fuzzy inference engine, fuzzy logic principles are used to combine the fuzzy IF-THEN rules in the fuzzy rule base into a mapping from the domain of input variables to the domain of output variables. Defuzzification is the process of converting a fuzzy demand of output variables into a crisp demand. After fuzzification, inference, and defuzzification procedures, each fuzzy controller will derive a proper control output, according to its corresponding inputs. In this study, five fuzzy sets (NB, NS, ZO, PS, and PB) are used for each input and output variables. Here N (negative), P (positive), S (small), B (Big), and ZO (zero) are used as abbreviations to represent each qualitative meaning. The triangle function is adopted as the membership function for each input and output variables, as shown in Fig. 6. The centroid defuzzifier is used to convert the control output obtained from the fired fuzzy rules to a real number [1, 2]. The fuzzy rules of the proposed three fuzzy controllers are shown in Tables 1 and 2.

The centroid method computes the center of gravity of the entire fuzzy command. The resulting real number, in some sense, summarizes the elastic constraint imposed on the possible value of the output variables by the fuzzy sets. Taking the anti-swing fuzzy controller as an example, the actual control output $u_{c,3}$, which sums up all the consequents parts of the

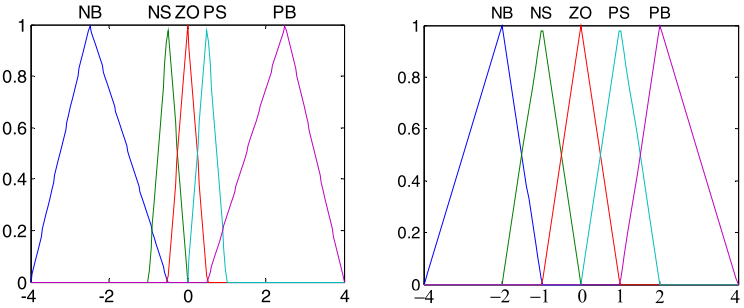

(a) Variables $E, EC, \widetilde{\alpha}, \widetilde{\dot{\alpha}}, u_{c,1}, u_{c,2}$ (b) Variables $u_{c,3}$

Fig. 6 Membership function of the fuzzy input and output variables

Table 1 Fuzzy control rules of trolley position fuzzy controller and trolley velocity fuzzy controller

Trolley position fuzzy controller						Trolley velocity fuzzy controller					
e	NB	NS	ZO	PS	PB	ec	NB	NS	ZO	PS	PB
$u_{c,1}$	NB	NS	ZO	PS	PB	$u_{c,2}$	NB	NS	ZO	PS	PB

Table 2 Fuzzy control rules of anti-swing fuzzy controller

$u_{c,3}$		α				
		NB	NS	ZO	PS	PB
$\dot{\alpha}$	NB	NB	NB	NB	NS	NB
	NS	NB	NS	NS	NS	NB
	ZO	NS	NS	ZO	PS	PS
	PS	PS	PS	PS	PS	PB
	PB	PB	PB	PB	PS	PB

fuzzy rules, can be given by

$$u_{c,3}(t) = \left(\sum_{j=1}^{25} q^j \min\left(\mu_{Aj}(\tilde{\alpha}), \mu_{Bj}(\tilde{\dot{\alpha}})\right)\right) \Big/ \left(\sum_{j=1}^{25} \min\left(\mu_{Aj}(\tilde{\alpha}), \mu_{Bj}(\tilde{\dot{\alpha}})\right)\right) \tag{35}$$

where μ_{Aj} and μ_{Bj} are the membership functions of α and $\dot{\alpha}$, respectively, and A^j and B^j are the fuzzy sets of α and $\dot{\alpha}$. q^j represents the greatest value of linguistic terms in the fuzzy set C^j of $u_{c,3}$.

3.2 Optimization of fuzzy controllers using genetic algorithms

The fuzzy controller described above was designed based on the intuition of the problem, and therefore, it could not work optimally due to the complex nature of the control problem. For example, the scale factors, quantization factors, and parameters of membership functions would greatly affect the stability and performance of the control system [28, 29]. In this section, GA technique [30–32] is employed to optimize the parameters of the fuzzy control

system offline, and here only the scale factors and the quantization factors are coded in a chromosome using a binary coding scheme:

$$X = (K_1, K_2, K_3, K_4, R_1, R_2, R_3). \tag{36}$$

Supposing $X^1, X^2, \ldots, X^{\text{pop}}$ as the N_{pop} individuals in the current population, letting $f_{g,1}(X^i) = \int e^2(t)\,\mathrm{d}t$, $f_{g,2}(X^i) = \int \alpha^2(t)\,\mathrm{d}t$, $f_{g,3}(X^i) = \int u_{C,x}^2(t)\,\mathrm{d}t$, and $h_{g,j}(X^i) = \max\{|f_{g,j}(X^1)|, |f_{g,j}(X^2)|, \ldots, |f_{g,j}(X^{\text{Npop}})|\}$, $(j = 1, 2, 3)$, the normalized object function can be defined as

$$g_{g,j}\big(X^i\big) = f_{g,j}\big(X^i\big)/h_{g,j}\big(X^i\big) \quad (j = 1, 2, 3). \tag{37}$$

Then the multi-objective optimization problem of controller parameters can be expressed as

$$\min\big\{g_{g,1}\big(X^i\big), g_{g,2}\big(X^i\big), g_{g,3}\big(X^i\big)\big\} \quad \big(X^i \in X \in R^7\big). \tag{38}$$

The point of this multi-objective optimization problem is to find all possible tradeoffs among multiple objective functions that are usually conflicting [30]. There are many genetic algorithms for solving a multi-objective optimization problem, and here the objective weighting method is adopted, which would transform a multi-objective optimization problem into a single objective optimization by defining the fitness function used to evaluate the status of each solution as

$$F\big(X^i\big) = w_{f,1}g_{g,1}\big(X^i\big) + w_{f,2}g_{g,2}\big(X^i\big) + w_{f,3}g_{g,3}\big(X^i\big) \tag{39}$$

where $w_{f,1}$, $w_{f,2}$, and $w_{f,3}$ are positive weight coefficients, which decide the weight proportion of each control objective in the comprehensive function (39), and finally affect the search direction of the optimal solution of multi-objective GA. In order to simplify the optimization algorithm, one can determine these target weight coefficients according to specific engineering experience directly. Since the search direction would be constant in the multi-dimensional objective space when a constant weight is assigned to each of the multiple objective functions, if engineering experience is lacking, one has to tentatively test the weight coefficients several times for obtaining a satisfactory optimization result [30]. In order to solve this problem, one can use the random weight [30] or adaptive weight [31] methods to change the weight coefficients, and achieve the various search directions in the multi-dimensional objective space. Taking the random weight method as an example, a random real number to each weight is assigned as follows when each pair of parent strings are selected for a crossover operation [30].

$$w_{f,j} = \text{rnd}_j / \sum_{k=1}^{3} \text{rnd}_k \quad (j = 1, 2, 3) \tag{40}$$

where rnd_j are non-negative random real numbers, which are generated for the weights $w_{f,1}$, $w_{f,2}$, and $w_{f,3}$ to calculate the weighted sum in (39) when each pair of parent strings is selected.

On the basis of defining the chromosomes (36) and fitness function (39), according to the GA, the initial population of chromosomes with a fixed number of random individuals from the whole solution space can be configured first. Then one can select a pair of highly adaptive individuals from the current population to produce new individuals for the next

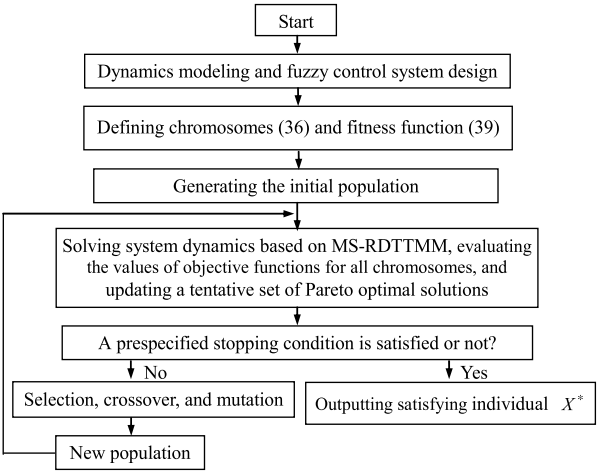

Fig. 7 Flow chart of offline parameters optimization by using GA based on the MS-RDTTMM

population by the roulette wheel method, in which the probability of choosing a certain individual is proportional to its fitness [20], that is,

$$\text{Prob}\left[X^i \text{ is selected}\right] = F\left(X^i\right) / \sum F\left(X^k\right). \tag{41}$$

This selection procedure is iterated $N_{\text{selection}}$ times in each generation for selecting $N_{\text{selection}}$ pairs of parent strings for a crossover operation [30]. If using the random weight [30] method, the weights $w_{f,1}$, $w_{f,2}$, and $w_{f,3}$ defined by Eq. (40) are not constant but variable at each of the $N_{\text{selection}}$ iterations, and the selection probability of each string is also variable even in a single generation, various search directions in the genetic algorithm could be realized.

The crossover and mutation are further applied to produce new children individuals and new generation. In order to avoid destroying optimal individuals in a genetic operation, the elitist preservation policy [30] could also be used. Repeating the above process until the number of generations reaches a specified maximum limit, the final set of Pareto optimal solutions will be obtained, form which a single optimal solution X^* can be selected by the decision maker's preference as the final solution. The flow chart of offline parameters optimization by using GA based on the MS-RDTTMM is shown in Fig. 7.

The computational cost of the above optimization process mainly depends on the population size, fitness evaluation efficiency, genetic operators efficiency (including selection, crossover, and mutation), and so on [20]. The fitness evaluation involves all individuals, and each evaluation needs to solve the system dynamics. As the proposed MS-RDTTMM has higher computational efficiency, under the same population size and genetic operators algorithms, the computational time of the parameter optimization process can be greatly reduced, that is, the proposed method is advantageous to the controller optimization design. It must be pointed out that the optimization solution and robustness of the optimization algorithm are closely related to both the maximum generation and population size. For any deterministic problem, when the population size is too small, even if the maximum generation is set very large, the entire optimization process is often prone to premature convergence and local optimum; with the increase of population size, the global search ability of the algorithm is relatively enhanced, the convergence algebra is smaller, and the robustness is also better. Therefore, in the implementation of the GA, the maximum generation and population

Table 3 Input values for the genetic algorithm used in optimization

Population size	70	Range of K_1	[0.05, 5]
Maximum generation	30	Range of K_1	[0.1, 10]
Generation gap	0.80	Range of K_3	[0.05, 5]
Crossover probability	0.65	Range of K_4	[0.1, 15]
Mutation probability	0.035	Range of R_1, R_2,R_3	[5, 200]

size should be set reasonably according to the problem complexity (the optimized parameter's number). The maximum number of generations and the population size are often set according to the experience, so far there is no specific method, and for different optimization problems one has different requirements. In this study, considering the computation efficiency and convergence, under the proper setting for the crossover and genetic probabilities, the population size is enough when setting it 8–12 times larger than the number of the optimized parameters, and the maximum number of generations in this case can be set to 30.

4 Numerical simulation

For the two-dimensional controlled overhead crane as shown in Fig. 1, the mass of the trolley, rope and load are $m_{\text{trolley}} = 30$ kg, $m_{\text{rope}} = 2.159$ kg, $m_{\text{load}} = 10$ kg, respectively. The length of rope is $l_{\text{rope}} = 3$ m, and the rope is divided into 50 rigid segments. The initial position of trolley is 0 m, and the initial swing angle of load is zero degrees. The control objective is to drive the trolley to transport the load safely from an initial position to the destination (18 m) in short time without residual swing. First of all, the above GA is used to optimize the parameters of the fuzzy control system designed in Sect. 3.1, the corresponding input values for the GA used in optimization are set as in Table 3. Then based on the optimized fuzzy controllers, the dynamics analysis of this system is presented by solving the transfer equation deduced by the proposed method and by directly integrating the global dynamic equations of the system deduced by Lagrange method [15], respectively.

The time history of the position of trolley obtained by the two methods is shown in Fig. 8. The time history of the swing angle of load obtained by the two methods is shown in Fig. 9. It can be seen clearly that the results obtained by the two methods have good agreement. The overshoot and steady state error of the trolley position are 0.55% and 0.065%, respectively. The maximal swing angle of the load is less than 0.09 rad during the trolley motion, and will go zero at time 11.5 s. The proposed method and control strategy guarantee not only prompt damping of the load swing but also accurate control of the crane position, and they achieve the trolley position tracking and anti-swing control perfectly. When dividing the rope into 50 rigid segments, a computational efficiency comparison of this dynamics simulation by the proposed and Lagrange methods (described by the global differential equation) [7, 15] under the same simulation platform is shown in Table 4. The ratio in Table 4 is equal to the CPU time of the involved method divided by the minimum CPU time of the two methods. It can be seen clearly that the calculated consumption ratio of the two methods is nearly 11.5:1, and the proposed method can greatly improve the calculation speed while keeping the accuracy.

With a gradual increase in the number of the rope segments, the computational stability of different methods is shown in Table 5. Compared with Lagrange method or ordinary MS-DT-TMM (see Eq. (25)), the proposed method has a lower matrix order, which means fewer computer storage requirements and the resulting higher computing efficiency. As the recursive multiplication of transfer matrices may lead to the propagation of round-off errors

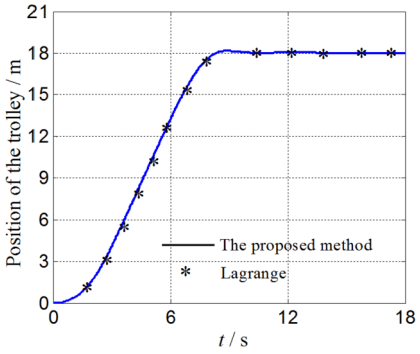

Fig. 8 Time history of the position of the trolley

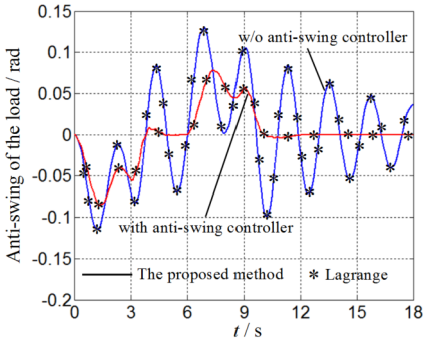

Fig. 9 Time history of the swing angle of the load

Table 4 Computational time comparison

Method	Lagrange method	The proposed method
Computational time ratio	11.491	1

by the ordinary MS-DTTMM (see Eq. Equation (25)), when the number of rope segments is large, the numerical instability of the ordinary MS-DTTMM would appear, which will have a negative impact on the computational accuracy and even cause the algorithm to become divergent or completely ineffective, as shown in Table 5. Once the algorithm diverges or becomes completely ineffective, it means computational failure ("F" in Table 5); otherwise the numerical calculation is stable ("S" in Table 5). In the proposed MS-RDTTMM, by introducing the Riccati transformation, the two-point boundary value problems which are numerically unstable can be transformed into initial value problems, and the system dynamics is solved by the recursive transfer equation (see Eq. (31)) instead of recursive multiplication of transfer matrices of elements, thus its numerical stability can be improved [33]. By using the proposed method, the computation result can be obtained even if the number of DOF of the system is more than 10 000.

5 Conclusions

In this paper, regarding the rope as a series of rigid segments connected by hinges, the multibody dynamic modeling and anti-swing control design of a two-dimensional overhead

Table 5 Contrast of computational stability and memory requirement

Number of rope segments	DOF of system	Method					
		Lagrange method		Ordinary MS-DT-TMM		The proposed method	
		System matrix order	Stability	System matrix order	Stability	System matrix order	Stability
5	7	7	S	7	S	3	S
12	14	14	S	7	S	3	S
50	52	52	S	7	F	3	S
80	82	82	S	7	F	3	S
200	202	202	S	7	F	3	S
500	502	502	S	7	F	3	S
1000	1002	1002	S	7	F	3	S
2000	2002	2002	S	7	F	3	S
5000	5002	5002	S	7	F	3	S
10 000	10 002	10 002	S	7	F	3	S

crane system is studied by using MS-RDTTMM. Three separate fuzzy logic controllers are designed for positioning and anti-swing control. For improving the performance of the fuzzy control system, a genetic algorithm based on the MS-RDTTMM is designed offline to tune the initial control parameters. The numerical verification is also carried out to show the computational efficiency, numerical stability, and control performance of the proposed method.

By using the recursive transfer formula to describe the system dynamics, instead of the global dynamics equation in ordinary dynamics methods, the matrices involved in this method are always very small, and the computational cost of dynamic analysis and control system optimization can be greatly reduced. In the illustrative simulation, when dividing the rope into 50 rigid segments, the calculated consumption ratio of the Lagrange and proposed method is nearly 11.5:1; and the proposed method can greatly improve the calculation speed while keeping the accuracy. In addition, by introducing the Riccati transformation, the numerical stability of the proposed method is substantially improved, which makes the application of the transfer matrix method to the large-scale multibody system dynamics possible.

In view of the importance of further practical test verification of the performance of the proposed fuzzy controller, the corresponding study on the experimental tests will be conducted in the following article.

Acknowledgements The research was supported by the Natural Science Foundation of China (Grant Nos. 11702292, 11605234).

References

1. Chang, C.Y.: Adaptive fuzzy controller of the overhead cranes with nonlinear disturbance. IEEE Trans. Ind. Inform. **3**(2), 164–172 (2007)
2. Chang, C.Y., Chiang, K.H.: Fuzzy projection control law and its application to the overhead crane. Mechatronics **18**, 607–615 (2008)
3. Matsuo, T., Yoshino, R., Suemitsu, H., et al.: Nominal performance recovery by PID+Q controller and its application to antisway control of crane lifter with visual feedback. IEEE Trans. Control Syst. Technol. **12**(1), 156–166 (2004)

4. Park, M.S., Chwa, D., Hong, S.K.: Antisway tracking control of overhead cranes with system uncertainty and actuator nonlinearity using an adaptive fuzzy sliding-mode control. IEEE Trans. Ind. Electron. **55**(11), 3972–3984 (2008)
5. Lee, H.H., Cho, S.K.: A new fuzzy-logic anti-swing control for industrial three-dimensional overhead cranes. In: Proceedings of IEEE International Conference on Robotics & Automation, pp. 2956–2961 (2001)
6. Karkoub, M.A., Zribi, M.: Modeling and energy based nonlinear control of crane lifters. IEE Proc., Control Theory Appl. **149**(3), 209–215 (2002)
7. Fang, Y., Dixon, W.E., Dawson, D.M., Zergeroglu, E.: Nonlinear coupling control laws for an underactuated overhead crane systems. IEEE/ASME Trans. Mechatron. **8**(3), 418–423 (2003)
8. Liu, D.T., Yi, J.Q., Zhao, D.B.: Adaptive sliding mode fuzzy control for a two-dimensional overhead crane. Mechatronics **15**, 505–522 (2005)
9. Yu, W., Moreno-Armendariz, M.A., Rodriguez, F.O.: Stable adaptive compensation with fuzzy CMAC for an overhead crane. Inf. Sci. **181**(21), 4895–4907 (2011)
10. Tuan, L.A., Moon, S.C., Lee, W.G., et al.: Adaptive sliding mode control of overhead cranes with varying cable length. J. Mech. Sci. Technol. **27**(3), 885–893 (2013)
11. Pezeshki, S., Badamchizadeh, M.A., Ghiasi, A.R., et al.: Control of overhead crane system using adaptive model-free and adaptive fuzzy sliding mode controllers. J. Control Autom. Electr. Syst. **26**(1), 1–15 (2015)
12. Zhang, Z.C., Wu, Y.Q., Huang, J.M.: Differential-flatness-based finite-time anti-swing control of underactuated crane systems. Nonlinear Dyn. **87**(3), 1749–1761 (2017)
13. Schiehlen, W.: Research trends in multibody system dynamics. Multibody Syst. Dyn. **18**(1), 3–13 (2007)
14. Wasfy, T.M., Noor, A.K.: Computational strategies for flexible multibody system. Appl. Mech. Rev. **56**(6), 553–613 (2003)
15. Shabana, A.A.: Dynamics of Multibody Systems. Cambridge University Press, New York (2005)
16. Ambrósio, J.A.C., Gonçalves, J.P.C.: Complex flexible multibody systems with application to vehicle dynamics. Multibody Syst. Dyn. **10**(6), 168–182 (2001)
17. Wittenburg, J.: Dynamics of Multibody Systems. Springer, Berlin (2008)
18. Pestel, E.C., Leckie, F.A.: Matrix Method in Elastomechanics. McGraw-Hill, New York (1963)
19. Rui, X.T., He, B., Lu, Y.Q., et al.: Discrete time transfer matrix method for multibody system dynamics. Multibody Syst. Dyn. **14**(3–4), 317–344 (2005)
20. Rong, B., Rui, X.T., Tao, L.: Dynamics and genetic fuzzy neural network vibration control design of a smart flexible four-bar linkage mechanism. Multibody Syst. Dyn. **28**(4), 291–311 (2012)
21. He, B., Rui, X.T., Wang, G.P.: Riccati discrete time transfer matrix method for elastic beam undergoing large overall motion. Multibody Syst. Dyn. **18**(4), 579–598 (2007)
22. Wang, G.P., Rong, B., Tao, L., et al.: Riccati discrete time transfer matrix method for dynamic modeling and simulation of an underwater towed system. J. Appl. Mech. **79**, 041014 (2012)
23. Rong, B.: Efficient dynamics analysis of large-deformation flexible beams by using the absolute nodal coordinate transfer matrix method. Multibody Syst. Dyn. **32**(4), 535–549 (2014)
24. Kamman, J.W., Huston, R.L.: Multibody dynamics modeling of variable length cable systems. Multibody Syst. Dyn. **5**, 211–221 (2001)
25. Williams, P., Trivailo, P.: A study on the transitional dynamics of a towed-circular aerial cable system. In: AIAA Atmospheric Flight Mechanics Conference and Exhibit, 15–18 August 2005, San Francisco, California (2005)
26. Quisenberry, J.E., Arena, A.S.: Discrete cable modeling and dynamic analysis. In: 44th AIAA Aerospace Sciences Meeting and Exhibit, 9–12 January 2006, Reno, Nevada (2006)
27. Dokainish, M.A., Subbaraj, K.: A study of direct time-integration methods in computational structural dynamics-I. Explicit methods. Comput. Struct. **32**(6), 1371–1386 (1989)
28. Zhou, Y.: Research and simulation on anti-swing of container crane using fuzzy intelligent control. Master's Thesis, Wuhan University of Technology (2003)
29. Wang, Y.Y.: Research on fuzzy logic anti-swing control of overhead crane. Master's Thesis, Dalian University of Technology (2008)
30. Murata, T., Ishibuchi, H., Tanaka, H.: Multi-objective genetic algorithm and its applications to flowshop scheduling. Comput. Ind. Eng. **30**(4), 957–968 (1996)
31. Li, Y., Liu, J.C., Wang, Y.: An improved adaptive weight approach GA for optimizing multi-objective rolling schedules in a tandem cold rolling. Control Theory Appl. **26**(6), 687–693 (2009)
32. Poursamad, A., Montazeri, M.: Design of genetic-fuzzy control strategy for parallel hybrid electric vehicles. Control Eng. Pract. **16**, 861–873 (2008)
33. Horner, G.C.: The Riccati transfer matrix method. Ph.D. dissertation, University of Virginia, USA (1975)